

Nonlinear Dynamic Modelling and Analysis of a 3-D Overhead Gantry Crane System with System Parameters Variation

R.M.T. Raja Ismail, M.A. Ahmad, M.S. Ramli, F.R.M. Rashidi

Faculty of Electrical and Electronics Engineering
Universiti Malaysia Pahang,
Pekan, 26600, Pahang, Malaysia

Abstract - Overhead cranes are widely used in industry for transportation of heavy loads. The natural sway of crane payloads is detrimental to safe and efficient operation. However, the crane acceleration, required for motion, always induces undesirable load swing. This paper presents dynamic modelling of a 3-D overhead gantry crane system based on closed-form equations of motion. The Lagrangian method is used to derive the dynamic model of the system. A dynamic model of the system incorporating payload and rope length is developed. Then the effects of payload and rope length on the response of the system are discussed. Extensive results that validate the theoretical derivation are presented in the time and frequency domains.

Keywords: 3-D overhead gantry crane, Lagrangian method, dynamic modelling, system parameters variation.

I. INTRODUCTION

A 3-D crane system is used frequently to move heavy cargo in factories and harbours. Overhead cranes have some serious problems, i.e. crane acceleration or deceleration always induces undesirable load swing. Disturbances, such as wind and rain, also decrease the crane performance by adversely affecting the crane control. Furthermore, a crane operator may not effectively control a crane due to carelessness or lack of experience. Such problems decrease the work efficiency and in some cases cause damage to the loads and cause safety accidents. Thus, an effective and precise crane motion control design is required for rapid and smooth automatic payload handling (Chang and Chiang, 2008). Therefore, research on the dynamic modelling of the gantry crane system is crucial before any controller can be implemented to the system.

Some studies developed the dynamic model and control design for 3-D overhead gantry crane system. The development of modelling and control method for a 3-D crane has been reported in Lee (1998). The employment of dynamic crane model to determine an optimal speed that minimized load swing has been investigated in Fang et al., (2003) and Piazzi and Visioli (2002). The modelling and energy based nonlinear control for crane lifters has been reported in Karkoub and Zribi (2002). In these studies, complex system dynamic equations for a crane must be considered for the controller. Anti-

swinging control and motion planning for 3-D gantry crane are also reported in Blajer and Kolodziejczyk (2007) and Garrido et al. (2008). Moreover, the study of the dynamic modelling of the other vibratory system incorporating payload is also has been reported. The study on the effects of payload on the dynamic behaviour of the 3-D gantry crane system has been presented in Ismail et al. (2009) and the investigation on the effects of payload on the dynamic behaviour of the two-link flexible manipulator system has been presented in Ahmad et al. (2008).

This paper presents a generalised modelling framework that provides a closed-form dynamic equation of motion of a 3-D overhead gantry crane system. The work also presents the effect of payloads on the dynamic behaviour of the system. The Euler-Lagrange principle is used to derive the dynamic model of the system. The simulation algorithm thus developed is implemented in Matlab. Cart position and swing angles of the system and the power spectral density (PSD) are obtained in both time and frequency domains. To study the effect of payloads and rope length, the results are evaluated with varying the two parameters of the gantry crane. Simulation results are analysed in both time and frequency domains to assess the accuracy of the model in representing the actual system.

The rest of this paper is structured in the following manner. The next section provides a brief description of the 3-D overhead gantry crane system considered in this

study. Section 3 describes the dynamic modelling of the system derived using Euler-Lagrange formulation. Simulation results with parameters variation are reported in Section 4. Finally, concluding remarks are offered in the last section.

II. THE 3-D OVERHEAD GANTRY CRANE SYSTEM

The 3-D overhead gantry crane system with its payload considered in this work is shown in Figure 1, where θ and ϕ denote the swing angles of the rope, L is the length of rope, and \mathbf{F} is the cart drive force.

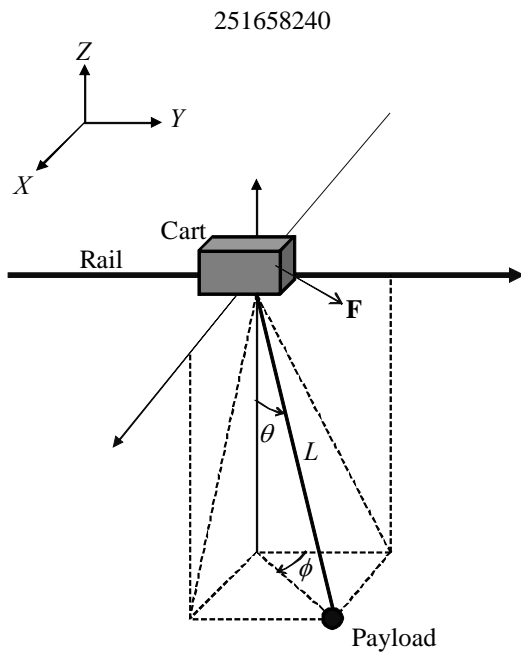


Figure 1 Description of the 3-D overhead gantry crane.

For simplicity, the cart friction force is ignored. The cart and the payload can be considered as point masses. The tension force that may cause the rope elongates is also ignored.

III. DYNAMIC MODELLING OF THE 3-D OVERHEAD GANTRY CRANE SYSTEM

This section provides detail description on the modelling of the 3-D overhead gantry crane system, as a basis of a simulation environment for the study on the effects of parameters variation to the system. The Euler-Lagrange formulation is considered in characterizing the dynamic behaviour of the crane system incorporate payload and length of the rope.

To derive the dynamic equations of motion of the 3-D overhead gantry crane system, the total energy associated with the crane system needs to be computed using the Lagrangian approach (Spong, 1997; Spong et al., 2006). Then, the Euler-Lagrange formulation is considered in characterizing the dynamic behaviour of the crane system.

Based on Figure 1, the rail, cart and payload position vectors are given by

$$\mathbf{r}_r = [x, 0, 0]$$

$$\mathbf{r}_c = [x, y, 0]$$

$$\mathbf{r}_p = [x + L \sin \theta \sin \phi, y + L \sin \theta \cos \phi, -L \cos \theta]$$

where x and y are the cart positions in X - and Y -directions respectively.

The total kinetic energy, \mathcal{K} and potential energy, \mathcal{P} of the whole system are given by

$$\mathcal{K} = \mathcal{K}_{\text{rail}} + \mathcal{K}_{\text{cart}} + \mathcal{K}_{\text{payload}}$$

$$\mathcal{P} = \mathcal{P}_{\text{payload}}$$

where

$$\mathcal{K}_{\text{rail}} = \frac{1}{2} m_r \dot{x}_r^2, \quad \mathcal{K}_{\text{cart}} = \frac{1}{2} m_c \dot{r}_c^2,$$

$$\mathcal{K}_{\text{payload}} = \frac{1}{2} m_p \dot{r}_p^2 + \frac{1}{2} J \dot{\theta}^2 + \frac{1}{2} J \dot{\phi}^2,$$

$$\mathcal{P}_{\text{payload}} = -m_p g L \cos \theta$$

where J denotes the moment of inertia of the payload and g is the gravity acceleration. Then, the total kinetic energy and the total potential energy are obtained as

$$\begin{aligned} \mathcal{K} = & \frac{1}{2} (m_p + m_r + m_c) \dot{x}^2 + \frac{1}{2} (m_p + m_c) \dot{y}^2 \\ & + m_p L \cos \theta \sin \phi \dot{x} \dot{\theta} + m_p L \sin \theta \cos \phi \dot{x} \dot{\phi} \\ & + m_p L \cos \theta \cos \phi \dot{y} \dot{\theta} - m_p L \sin \theta \sin \phi \dot{y} \dot{\phi} \end{aligned} \quad (1)$$

$$+ \frac{1}{2} (m_p L^2 + J) \dot{\theta}^2 + \frac{1}{2} (m_p L^2 \sin^2 \theta + J) \dot{\phi}^2$$

$$\mathcal{P} = -m_p g L \cos \theta \quad (2)$$

Using the Lagrangian approach, the Lagrangian of the system is obtain as

$$\mathcal{L} = \mathcal{K} - \mathcal{P} \quad (3)$$

Then, the Euler-Lagrange formulation is used that is

$$\frac{d}{dt} \left(\frac{\partial \mathcal{L}}{\partial \dot{q}_i} \right) - \frac{\partial \mathcal{L}}{\partial q_i} = F_i, \quad i = 1, 2, 3, 4. \quad (4)$$

where \mathbf{q} is the state vector and \mathbf{F} is the control vector which are defined as

$$\mathbf{q} = [x \quad y \quad \theta \quad \phi]^T$$

$$\mathbf{F} = [f_x \quad f_y \quad 0 \quad 0]^T$$

where f_x and f_y denote the control force inputs acting on the X - and Y -direction motions. From (4), a set of four equations is obtained that is

$$\frac{d}{dt} \left(\frac{\partial \mathcal{L}}{\partial \dot{x}} \right) - \frac{\partial \mathcal{L}}{\partial x} = f_x, \quad \frac{d}{dt} \left(\frac{\partial \mathcal{L}}{\partial \dot{y}} \right) - \frac{\partial \mathcal{L}}{\partial y} = f_y$$

$$\frac{d}{dt} \left(\frac{\partial \mathcal{L}}{\partial \dot{\theta}} \right) - \frac{\partial \mathcal{L}}{\partial \theta} = 0, \quad \frac{d}{dt} \left(\frac{\partial \mathcal{L}}{\partial \dot{\phi}} \right) - \frac{\partial \mathcal{L}}{\partial \phi} = 0$$
(5)

From (5), the dynamic model of the 3-D overhead gantry crane system can be expressed in the form of matrices such that

$$\mathbf{M}(\mathbf{q})\ddot{\mathbf{q}} + \mathbf{C}(\mathbf{q}, \dot{\mathbf{q}})\dot{\mathbf{q}} + \mathbf{G}(\mathbf{q}) = \mathbf{F} \quad (6)$$

where the matrices $\mathbf{M}(\mathbf{q}) \in \mathfrak{R}^{4 \times 4}$, $\mathbf{C}(\mathbf{q}, \dot{\mathbf{q}}) \in \mathfrak{R}^{4 \times 4}$, and $\mathbf{G}(\mathbf{q}) \in \mathfrak{R}^4$ represent the inertia, Centripetal-Coriolis terms, and gravity, respectively, and are defined as

$$\mathbf{M}(\mathbf{q}) = \begin{bmatrix} m_p + m_r + m_c & 0 & & \\ 0 & m_p + m_c & & \\ m_p L \cos \theta \sin \phi & m_p L \cos \theta \cos \phi & & \\ m_p L \sin \theta \cos \phi & -m_p L \sin \theta \sin \phi & & \\ & m_p L \cos \theta \sin \phi & m_p L \sin \theta \cos \phi & \\ & m_p L \cos \theta \cos \phi & -m_p L \sin \theta \sin \phi & \\ & m_p L^2 + J & 0 & \\ & 0 & m_p L^2 \sin^2 \theta + J & \end{bmatrix} \quad (7)$$

$$\mathbf{C}(\mathbf{q}, \dot{\mathbf{q}}) = \begin{bmatrix} 0 & 0 & -m_p L \sin \theta \sin \phi \dot{\theta} + m_p L \cos \theta \cos \phi \dot{\phi} & \\ 0 & 0 & -m_p L \sin \theta \cos \phi \dot{\theta} - m_p L \cos \theta \sin \phi \dot{\phi} & \\ 0 & 0 & 0 & \\ 0 & 0 & m_p L^2 \sin \theta \cos \theta \dot{\theta} & \\ & m_p L \cos \theta \cos \phi \dot{\theta} - m_p L \sin \theta \sin \phi \dot{\phi} & & \\ & -m_p L \cos \theta \sin \phi \dot{\theta} - m_p L \sin \theta \cos \phi \dot{\phi} & & \\ & -m_p L^2 \sin \theta \cos \theta \dot{\theta} & & \\ & m_p L^2 \sin \theta \cos \theta \dot{\theta} & & \end{bmatrix} \quad (8)$$

$$\mathbf{G}(\mathbf{q}) = [0 \quad 0 \quad m_p g L \sin \theta \quad 0]^T \quad (9)$$

After rearranging (6) and multiplying both sides by \mathbf{M}^{-1} , one obtains

$$\ddot{\mathbf{q}} = \mathbf{M}^{-1}(-\mathbf{C}\dot{\mathbf{q}} - \mathbf{G} + \mathbf{F}) \quad (10)$$

where \mathbf{M}^{-1} is guaranteed to exist due to $\det(\mathbf{M}) > 0$. From (10), the swing angles of the payload with respect to YZ -plane, θ_x and with respect to XZ -plane, θ_y are obtained as

$$\theta_x = \tan^{-1}(\tan \theta \sin \phi)$$

$$\theta_y = \sin^{-1}(\sin \theta \cos \phi)$$

In this study, the nominal values of the parameters are defined as $m_p = 0.73$ kg, $m_c = 1.06$ kg, $m_r = 6.4$ kg, $L = 0.7$ m and $J = 0.005$ kg-m² (Chang and Chiang, 2008). In order to investigate the dynamic behaviour of the system incorporating payload, m_p is varied from 0 to 1 kg while L is set to its nominal value. On the other hand, to study the effect of the rope length to the dynamic behaviour of the system, the value of L is varied from 0 to 1 m while m_p is set to its nominal. The value of gravity acceleration is $g = 9.8$ m-s⁻².

IV. SIMULATION RESULTS

In this section, simulation results of the dynamic behaviour of the 3-D overhead gantry crane system are presented in the time and frequency domains. A bang-bang signal of amplitude 1 N and 1 s width is used as an input force, applied at the cart of the gantry crane. A bang-bang force has a positive (acceleration) and negative (deceleration) period allowing the cart to, initially, accelerate and then decelerate and eventually stop at a target location.

System responses are verified by undertaking computer simulation using the fourth-order Runge-Kutta integration method for duration of 20 s with a sampling time of 1 ms. The swing angles responses of the system with the power spectral density (PSD) are obtained and evaluated.

A. System Responses with Payload Variation

To demonstrate the effects of payload on the dynamic behaviour of the system, various payloads of up to 1 kg weight were simulated. Figure 2 and Figure 3 show the responses of the cart positions in X - and Y -directions, respectively for various payloads. It is noted that the average final positions for both X - and Y -directions of the cart decrease. Moreover, the chattering of the final position response varies from 3 to 7 mm for position in X -direction and 2.2 to 3.6 cm for position in Y -direction.

Table 1 summarizes the relation between payload and the cart position response. Figure 4 and Figure 5 respectively show the swing angles with respect to *YZ*- and *XZ*-planes responses, with various payloads. It is shown that the oscillations of the swing angles decrease with increasing payloads. The relation between payload and the swing angles is also shown in Table 1. Figure 6 and Figure 7 show the corresponding PSDs for both swing angles. It demonstrates that the resonance modes of vibration of the system shift to higher frequencies with increasing payloads. Table 2 summarizes the relation between payload and the resonance frequencies of the system. This study shows that, in order to decrease the oscillation of the system, a same control design can be used for several systems although they have different payloads. This result is remarkable since the parameters of a controller do not need to be redesigned if the payload is varied within the specific range.

251658240

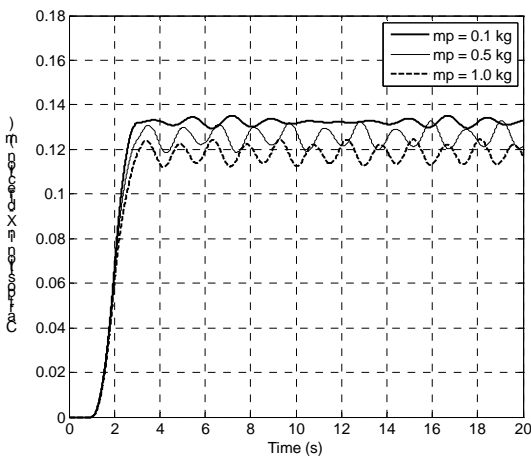


Figure 2 Position of the cart in *X*-direction with variation of m_p .
251658240

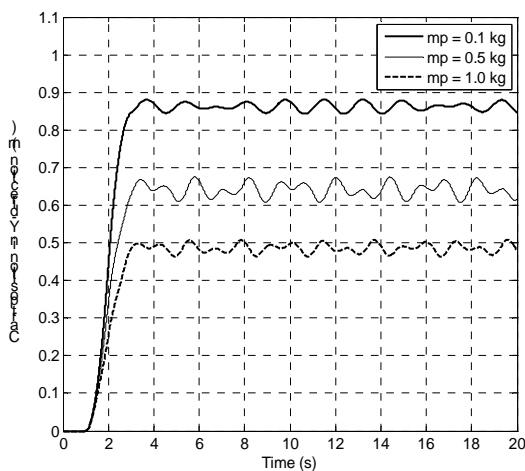


Figure 3 Position of the cart in *Y*-direction with variation of m_p .

251658240

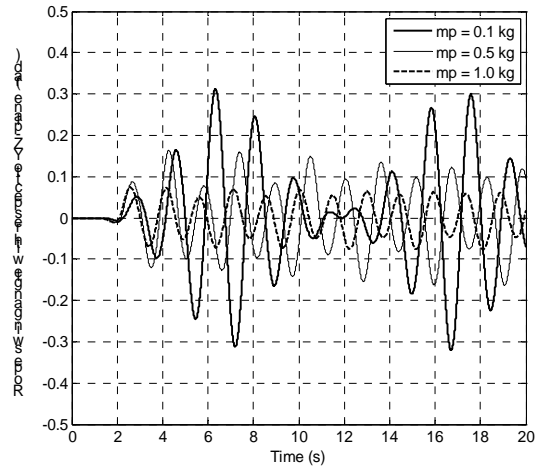


Figure 4 Swing angle of the rope with respect to *YZ*-plane with variation of m_p .

251658240

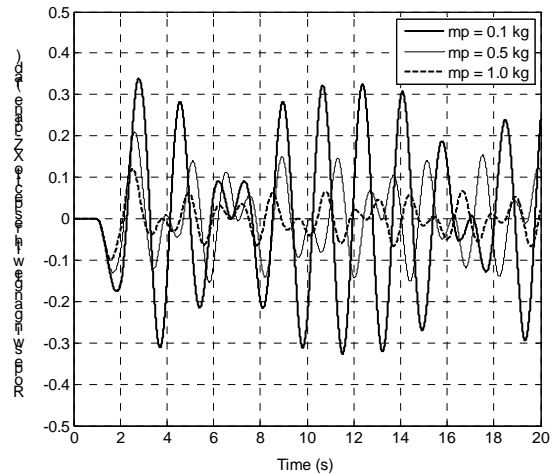


Figure 5 Swing angle of the rope with respect to *XZ*-plane with variation of m_p .

Table 1: Relation between payload mass with cart position and swing angles responses.

Payload mass (kg)	Cart position (m)				Swing angles (rad)	
	X-direction		Y-direction		With respect to YZ-plane, θ_x	With respect to XZ-plane, θ_y
	Average	Oscillation	Average	Oscillation		
0	0.1340	-	0.9434	-	0	0
0.1	0.1321	± 0.0031	0.8455	± 0.0359	± 0.3202	± 0.3400
0.2	0.1301	± 0.0049	0.7936	± 0.0297	± 0.2711	± 0.3002
0.3	0.1289	± 0.0061	0.7353	± 0.0347	± 0.2266	± 0.2660
0.4	0.1272	± 0.0069	0.6849	± 0.0357	± 0.1949	± 0.2361
0.5	0.1257	± 0.0072	0.6425	± 0.0328	± 0.1631	± 0.2099
0.6	0.1243	± 0.0072	0.6032	± 0.0329	± 0.1407	± 0.1869
0.7	0.1223	± 0.0073	0.5683	± 0.0304	± 0.1204	± 0.1668
0.8	0.1211	± 0.0070	0.5377	± 0.0278	± 0.1033	± 0.1492
0.9	0.1198	± 0.0065	0.5101	± 0.0251	± 0.0887	± 0.1337
1.0	0.1184	± 0.0062	0.4862	± 0.0221	± 0.0769	± 0.1201

251658240

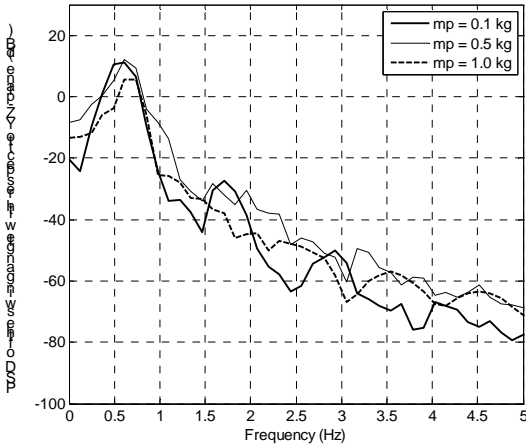


Figure 6 Power spectral density of the swing angle with respect to YZ-plane with variation of m_p .

251658240

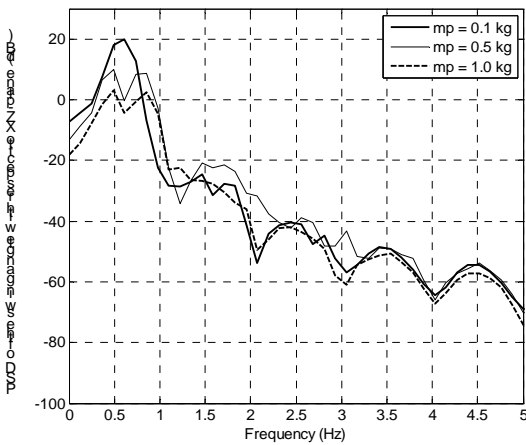


Figure 7 Power spectral density of the swing angle with respect to XZ-plane with variation of m_p .

Table 2: Relation between payload and resonance frequencies of the 3-D overhead gantry crane system.

Payload (kg)	Resonance frequency (Hz)			
	Swing angle θ_x		Swing angle θ_y	
	Mode 1	Mode 2	Mode 1	Mode 2
0	-	-	-	-
0.1	0.4883	1.7090	0.6104	1.4650
0.2	0.4883	1.8310	0.6104	1.5870
0.3	0.6104	1.8310	0.7324	1.5870
0.4	0.6104	1.8310	0.7324	1.7090
0.5	0.6104	1.9530	0.7324	1.7090
0.6	0.7324	1.9530	0.8545	1.8310
0.7	0.7324	1.9530	0.8545	1.8310
0.8	0.7324	2.0750	0.8545	1.8310
0.9	0.7324	2.0750	0.8545	1.9530
1.0	0.7324	2.0750	0.8545	1.9530

B. System Responses with Rope Length Variation

Similarly, to demonstrate the effects of rope length on the dynamic behaviour of the system, various length of rope up to 1 m were simulated. Figure 8 and Figure 9 show the responses of the cart positions in X- and Y-directions, respectively for various rope lengths. Remarkably, the variation of the rope length does not affect much on the average final positions for both X- and Y-directions. However, the chattering of the final position response varies from 0.5 to 13 mm for position in X-direction and 0.9 to 6 cm for position in Y-direction. Table 3 summarizes the relation between rope length and the cart position response. Figure 10 and Figure 11 respectively show the swing angles with respect to YZ- and XZ-planes responses, with various rope lengths. It is

shown that, apart from rope length 0.1 m and 0.2 m, the oscillations of the swing angles increase with increasing rope length. The relation between rope length and the swing angles is also shown in Table 3. Figure 12 and Figure 13 show the corresponding PSDs for both swing angles. It demonstrates that the resonance modes of vibration of the system shift to higher frequencies with increasing rope length. Table 4 summarizes the relation between rope length and the resonance frequencies of the system. This investigation shows that, a similar control design can be used for several systems although they have different rope length, in order to reduce the oscillation of the system. This result is also significant since one does not have to redesign a controller if the rope length is varied within the specific range.

251658240

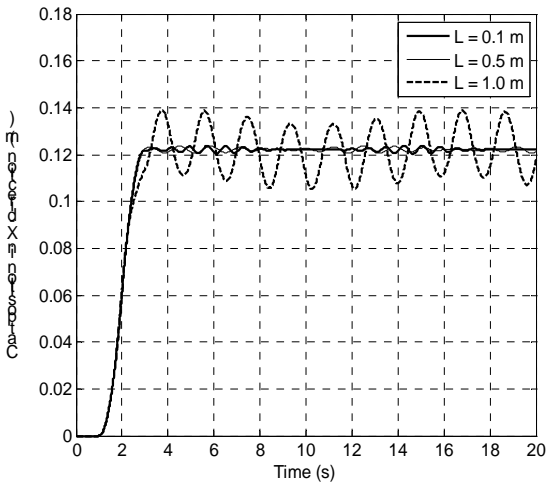


Figure 8 Position of the cart in X -direction with variation of L .
251658240

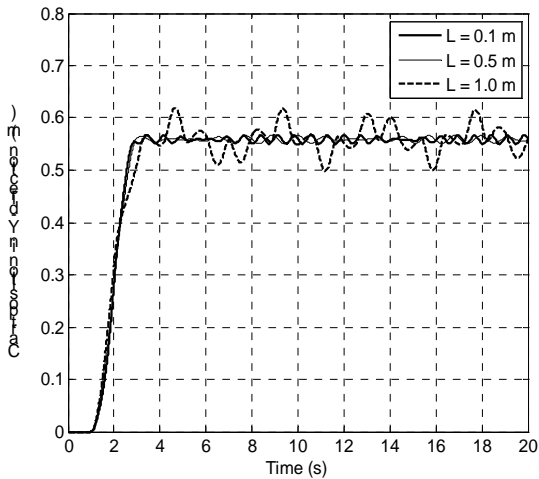


Figure 9 Position of the cart in Y -direction with variation of L .

251658240

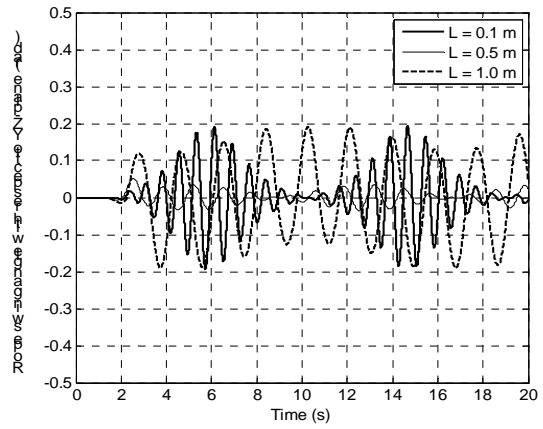


Figure 10 Swing angle of the rope with respect to YZ -plane with variation of L .
251658240

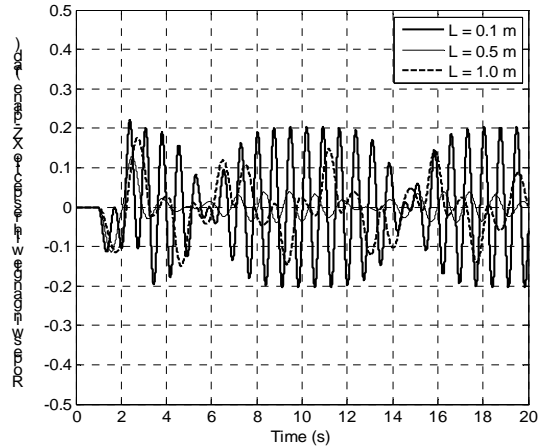


Figure 11 Swing angle of the rope with respect to XZ -plane with variation of L .
251658240

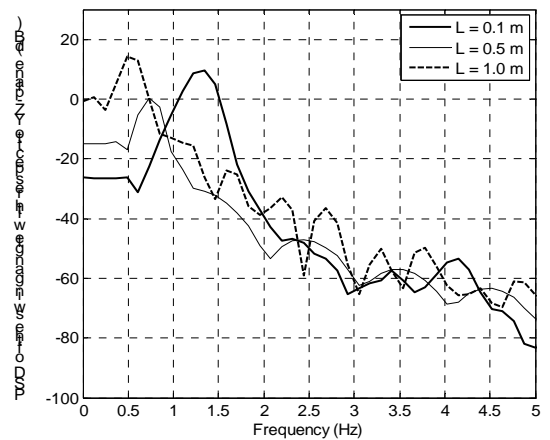


Figure 12 Power spectral density of the swing angle with respect to YZ -plane with variation of L .

Table 3: Relation between rope length with cart position and swing angles responses.

Rope length (m)	Cart position (m)				Swing angles (rad)	
	X-direction		Y-direction		With respect to YZ-plane, θ_x	With respect to XZ-plane, θ_y
	Average	Oscillation	Average	Oscillation		
0	-	-	-	-	-	-
0.1	0.1222	± 0.0005	0.5580	± 0.0089	± 0.1904	± 0.2045
0.2	0.1273	± 0.0005	0.5657	± 0.0088	± 0.1885	± 0.1907
0.3	0.1235	± 0.0007	0.5644	± 0.0085	± 0.0190	± 0.0108
0.4	0.1300	± 0.0008	0.5673	± 0.0087	± 0.0243	± 0.0169
0.5	0.1266	± 0.0010	0.5586	± 0.0085	± 0.0519	± 0.0387
0.6	0.1245	± 0.0035	0.5669	± 0.0188	± 0.0795	± 0.0605
0.7	0.1303	± 0.0058	0.5620	± 0.0289	± 0.1072	± 0.0824
0.8	0.1230	± 0.0083	0.5594	± 0.0390	± 0.1346	± 0.1041
0.9	0.1300	± 0.0106	0.5677	± 0.0494	± 0.1623	± 0.1250
1.0	0.1269	± 0.0131	0.5658	± 0.0597	± 0.1899	± 0.1475

251658240

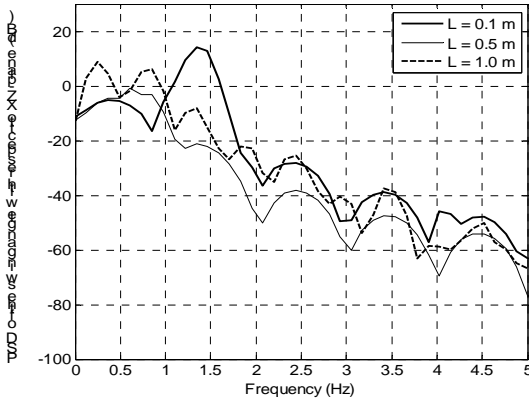


Figure 13 Power spectral density of the swing angle with respect to XZ-plane with variation of L .

Table 4: Relation between rope length and resonance frequencies of the 3-D overhead gantry crane system.

Rope length (kg)	Resonance frequency (Hz)			
	Swing angle θ_x		Swing angle θ_y	
	Mode 1	Mode 2	Mode 1	Mode 2
0	-	-	-	-
0.1	1.343	4.150	1.343	2.441
0.2	1.221	3.906	1.099	2.197
0.3	1.099	3.418	0.9766	1.953
0.4	0.9766	2.930	0.7324	1.587
0.5	0.7324	2.441	0.6104	1.343
0.6	0.7324	2.197	0.6104	1.221
0.7	0.6104	2.075	0.4883	1.099
0.8	0.6104	1.953	0.3662	0.9766
0.9	0.4883	1.831	0.3662	0.8545
1.0	0.4883	1.587	0.2441	0.8545

V. CONCLUSION

Investigation into the development of a dynamic model of a 3-D gantry crane system incorporating payload and rope length has been presented. A closed-form finite dimensional dynamic model of the system has been developed using the Euler-Lagrange approach. The derived dynamic model has been simulated with bang-bang force input. The cart position and swing angle responses of the gantry system have been obtained and analysed in time and frequency domains. Moreover, the effects of payload and rope length on the dynamic characteristic of the system have been studied and discussed. These results are very helpful and important in the development of effective control algorithms for a 3-D gantry crane system with variation of payload and rope length.

REFERENCES

- [1] Ahmad, M.A., Mohamed, Z. and Hambali, N. (2008). Dynamic Modelling of a Two-link Flexible Manipulator System Incorporating Payload. 3rd IEEE Conference on Industrial Electronics and Applications, pp. 96-101.
- [2] Blajer, W. and Kolodziejczyk, K. (2007). Motion Planning and Control of Gantry Cranes in Cluttered Work Environment. IET Control Theory Applications, Vol. 1, No. 5, pp. 1370-1379.
- [3] Chang, C.Y. and Chiang, K.H. (2008). Fuzzy Projection Control Law and its Application to the Overhead Crane. Journal of Mechatronics, Vol. 18, pp. 607-615.
- [4] Fang, Y., Dixon, W.E., Dawson, D.M. and Zergeroglu, E. (2003). Nonlinear Coupling Control Laws for an Underactuated Overhead Crane System. IEEE/ASME Trans. on Mechatronics, Vol. 8, No. 3, pp. 418-423.
- [5] Garrido, S., Abderrahim, M., Gimenez, A., Diez, R. and Balaguer, C. (2008). Anti-Swinging Input Shaping Control of an Automatic Construction Crane. IEEE Trans. on Automation Science and Engineering, Vol. 5, No. 3, pp. 549-557.
- [6] Ismail, R.M.T.R., Ahmad, M.A., Ramli, M.S. and Rashidi, F.R.M. (2009). Nonlinear Dynamic Modelling and Analysis of a 3-D

- Overhead Gantry Crane System with Payload Variation. Third UKSim European Symposium on Computer Modeling and Simulation, pp. 350-354.
- [7] Karkoub, M.A. and Zribi, M. (2002). Modelling and Energy Based Nonlinear Control of Crane Lifters. IEE Proc. Control Theory Application, Vol. 149, No. 3, pp. 209-216.
- [8] Lee, H.H. (1998). Modeling and Control of a Three-Dimensional Overhead Crane. Journal of Dynamics Systems, Measurement, and Control, Vol. 120, pp. 471-476.
- [9] Piazzzi, A. and Visioli, A. (2002). Optimal Dynamic-inversion-based Control of an Overhead Crane. IEE Proc. Control Theory Application, Vol. 149, No. 5, pp. 405-411.
- [10] Spong, M.W. (1997). Underactuated Mechanical Systems, Control Problems in Robotics and Automation. London: Springer-Verlag.
- [11] Spong, M.W., Hutchinson, S. and Vidyasagar, M. (2006). Robot Modeling and Control. New Jersey: John Wiley.